

Scheme and Experimental Demonstration of Fully Atomic Weak Value Amplification

Chun-Wang Wu,^{1,2,*} Jie Zhang,^{1,2,*} Yi Xie,^{1,2} Bao-Quan Ou,^{1,2} Ting Chen,^{1,2} Wei Wu,^{1,2,†} and Ping-Xing Chen^{1,2,‡}

¹*Department of Physics, College of Liberal Arts and Sciences, National University of Defense Technology, Changsha 410073, Hunan, China.*

²*Interdisciplinary Center for Quantum Information, National University of Defense Technology, Changsha 410073, Hunan, China.*

(Dated: June 21, 2019)

In this Letter, we explore the possibilities of realizing weak value amplification (WVA) using purely atomic degrees of freedom. Our scheme identifies the internal electronic states and external motional states of a single trapped $^{40}\text{Ca}^+$ ion as the system degree and pointer degree respectively, and their controllable weak coupling is provided by a bichromatic light field. In our experimental demonstration, by performing appropriate postselection on the internal states, a tiny position displacement of $\sim 4 \text{ \AA}$ of the trapped ion is amplified to $\sim 10 \text{ nm}$. The extreme sensitivity of the amplification effect to the relative phase of the quantum state is also demonstrated, which may have relation to the phase estimation applications. This work has potential to advance the abundant metrological applications related to the atomic interferometric process, and allows fully exploration of the peculiarities of WVA owing to the high operational flexibility of this procedure.

PACS numbers: 03.65.Ta, 39.20.+q, 06.20.Dk, 42.50.Ct

Quantum measurement lies at the heart of quantum mechanics, and its peculiar properties have perplexed physicists for almost one century [1]. In 1932, von Neumann proposed a phenomenological model which describes quantum measurement as an interaction process between two quantum systems (or two quantum degrees of one system), regarded as “measured system” and “measuring pointer” respectively [2]. Then in 1988, Aharonov, Albert and Vaidman (AAV) extended von Neumann’s measurement model from the regular strong measurement regime to the weak measurement regime, corresponding to the cases where the system and pointer interact strongly and weakly, respectively [3]. They showed that, if an appropriate postselection step is introduced into the weak measurement procedure, the measured value (defined by AAV as “weak value”) may lie outside the eigenvalue spectrum of the observable in question, giving rise to the so-called “weak value amplification (WVA)” effect. In recent years, WVA has been proven to be useful as an amplification technique for observing the extreme weak physical effect, quantum state tomography, tests of quantum mechanics paradoxes and so on [4, 5].

In virtue of the high-level manipulation and mature detection techniques for photons, WVA has made great development in the linear optical system both in theoretical and experimental aspects. Up to now, optical WVA technique has been successfully applied to the observation of the spin Hall effect of light [6], the ultrasensitive measurement of the light beam deflection [7], the amplification of optical nonlinearities [8], the direct tomography of photonic quantum states [9], the clarification of controversial debates in quantum mechanics [10], and the counteraction of decoherence in the quantum optical

system [11]. Although WVA cannot overcome the shot-noise-limit imposed by quantum mechanics [12, 13], some references claimed that this amplification technique may offer substantial improvements in many practical cases where certain types of technical noise and operational limitations dominate [14–19].

Recently, much effort has been expended in attempts to realize WVA in at least partially nonphotonic systems [20–27]. Among these works, exploration of WVA in cold atoms or trapped ions is particularly interesting for two reasons. First of all, atomic WVA technique has potential to advance the abundant metrological applications related to the atomic interferometric process, e.g. the atomic clock [28] and the atomic magnetometer [29]. Secondly, compared with optical WVA which can be usually explained using classical optics [30], atomic WVA is a purely quantum effect and is more suitable to verify the peculiarities of quantum mechanics. In 2013, Shomroni *et al.* demonstrated WVA based on atomic spontaneous emission [25]. However, the involving atomic ensemble only plays the role of light source in their procedure and it is still an optical WVA experiment in essence. More recently, Ref. [26] presented a WVA proposal based on atomic matter wave interferometry, but the requirement for accurate manipulation and detection of the external orbital motions of free atoms makes it difficult to perform in experiment. Then in 2019, Araneda *et al.* performed WVA based on spontaneous emission of a single trapped ion to calibrate the wavelength-scale errors in optical localization [27]. To the best of our knowledge, the experimental demonstration of WVA using purely atomic degrees of freedom has not been realized so far.

In this Letter, we present the first proof-of-principle experimental demonstration of purely atomic WVA us-

ing a single trapped $^{40}\text{Ca}^+$ ion. For our experiment, the internal electronic states and the external motional states of the ion play the roles of the measured system and the measuring pointer, respectively. With the help of spin-dependent displacement, heralded measurement and motional wavepacket reconstruction techniques well established in the trapped ion system, we achieve an effective amplification factor as large as 25 for the position displacement of the ion. We also show that WVA is extremely sensitive to the relative phase of the quantum state. We believe that this work opens up the interesting possibility to explore WVA in atomic interferometric techniques.

The WVA formalism can be briefly outlined based on von Neumann's measurement model [3]. A quantum system, with its observable \hat{A} being measured, is coupled to a measuring pointer by an interaction Hamiltonian $\hat{H} = g\delta(t - t_0)\hat{A}\hat{p}$, where \hat{p} is the canonical momentum of the pointer (with conjugate position \hat{q}), g is the interaction strength, t is the time variable, and $\delta(t - t_0)$ is the impulse function centered at the time t_0 satisfying $\int_{-\infty}^{\infty} \delta(t - t_0)dt = 1$. Suppose the measured system is prepared in the state $|\psi_i\rangle = \sum_m \alpha_m |a_m\rangle$, where $|a_m\rangle$ is the eigenstate of \hat{A} with the corresponding eigenvalue a_m , and the measuring pointer is initialized in $|\varphi(q)\rangle$, where q is the position variable. Under the action of the unitary evolution operator $\hat{U} = \exp(-ig\hat{A}\hat{p}/\hbar)$, the combined state will evolve into $\sum_m \alpha_m |a_m\rangle |\varphi(q - a_m g)\rangle$. In the weak coupling limit where g is so small that \hat{U} needs only to be expanded to first order in perturbation theory, if we introduce a postselection step by performing a projective measurement on the system and retaining only instances with given outcome $|\psi_f\rangle$, the pointer will be left in the state

$$\begin{aligned} \langle\psi_f|\hat{U}|\psi_i\rangle|\varphi(q)\rangle &\approx \langle\psi_f|(1 - ig\hat{A}\hat{p}/\hbar)|\psi_i\rangle|\varphi(q)\rangle \\ &= \langle\psi_f|\psi_i\rangle(1 - iA_w g\hat{p}/\hbar)|\varphi(q)\rangle \\ &\approx \langle\psi_f|\psi_i\rangle \exp(-iA_w g\hat{p}/\hbar)|\varphi(q)\rangle \\ &= \langle\psi_f|\psi_i\rangle|\varphi(q - A_w g)\rangle, \end{aligned} \quad (1)$$

where

$$A_w \equiv \langle\psi_f|\hat{A}|\psi_i\rangle / \langle\psi_f|\psi_i\rangle \quad (2)$$

is the weak value defined by AAV. It is easy to note that, under the condition of $|\langle\psi_f|\psi_i\rangle| \ll 1$, the pointer shift is "amplified" because $|A_w| \gg \max_m \{|a_m|\}$ and the so-called WVA effect arises. It can be shown from Eq. (2) that the weak value A_w may be an imaginary number. For the imaginary WVA, Ref. [31] showed that we can observe an amplified shift in the momentum direction with the same interaction Hamiltonian above.

Our scheme of WVA in a single trapped ion can be simply illustrated in Fig. 1(a). Firstly, a pseudo-spin, composed of two internal electronic states of the ion

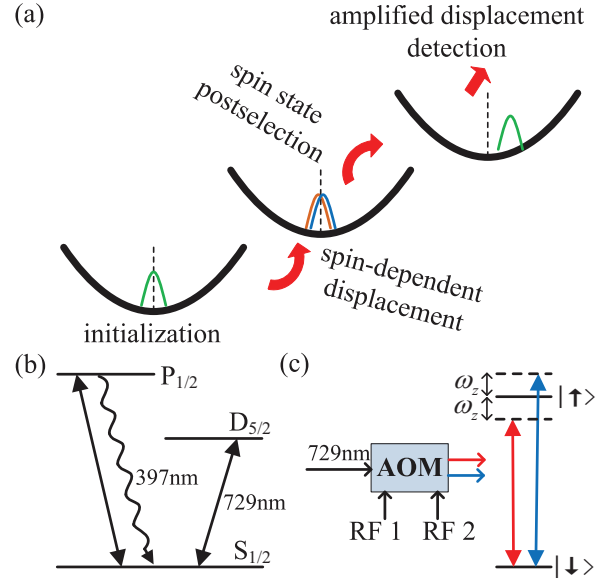


FIG. 1. (Color online) (a) Schematic illustration of WVA effect in a single trapped $^{40}\text{Ca}^+$ ion. (b) The internal electronic states and coupling lasers used for coherent manipulation and projective measurement in our experiment. (c) Configuration of the bichromatic light field used for spin-dependent displacement.

and used as the system degree, is prepared in the superposition of the eigenstates of one system observable being measured. The external motion of the ion, used as the pointer degree, is initialized to the ground state wavepacket. Then, a weak spin-dependent force displaces the motional wavepacket towards opposite directions for different eigenstates of the system observable. Finally, by performing the projective measurement of another system observable and retaining the postselected outcome, the original tiny splitting of the wavepacket may be changed to a large displacement towards a certain direction in phase space. This striking amplification effect essentially results from the constructive quantum interference in the tail of the splitted wavepackets and destructive interference elsewhere. While introduced as a model of the measurement of a system observable, this procedure is usually used as an amplification method for the tiny interaction between the system degree and the pointer degree.

In the experiment, we use a single $^{40}\text{Ca}^+$ ion trapped in a blade-shaped linear Paul trap with radial and axial trapping frequencies $\omega_r = 2\pi \times 1.6$ MHz and $\omega_z = 2\pi \times 1.41$ MHz, respectively. Fig. 1(b) shows the relevant internal levels and coupling lasers used for coherent manipulation and projective measurement (more details on the experimental configuration can be found in Supplemental Material). The Zeeman sublevels $S_{1/2}(m_J = -1/2)$ and $D_{5/2}(m_J = -1/2)$ in a magnetic field of 5.3 G are identified as the spinor states $|\downarrow\rangle$ and $|\uparrow\rangle$ respectively, the

optical quadrupole transition between which is driven by a narrow linewidth laser at 729 nm. The 729 nm laser beam enters the trap by passing through two hollow end-cap electrodes with an angle of 0° to the axial z direction, resulting in a Lamb-Dicke parameter of $\eta \simeq 0.08$. The spinor state measurement is done via state-dependent fluorescence observed while coupling the $S_{1/2}$ state to the short-lived state $P_{1/2}$ (with lifetime 7.1 ns) using a laser field at 397 nm. The external motional degree we use for the experiment is the axial mode of the motion, which can be treated as a quantum mechanical harmonic oscillator with a frequency of ω_z . Its ground-state wavepacket has the size of $\Delta_z = \sqrt{\hbar/2m\omega_z} \simeq 9.47$ nm, where m is the ion's mass.

The spin-dependent displacement is implemented using a bichromatic light field resonant with both the blue and red axial sidebands of the $|\downarrow\rangle \leftrightarrow |\uparrow\rangle$ transition, which is realized by sending the 729 nm laser field through an acousto-optic modulator (AOM) driven with two frequencies of RF signals that differ by $2\omega_z$ (see Fig. 1(c)). In the Lamb-Dicke regime, the resulting Hamiltonian reads

$$\hat{H}_d = \frac{\hbar\eta\Omega}{2} [\hat{\sigma}_x \sin \phi_+ + \hat{\sigma}_y \cos \phi_+] \otimes [-(\hat{a}^\dagger + \hat{a}) \cos \phi_- + i(\hat{a}^\dagger - \hat{a}) \sin \phi_-], \quad (3)$$

where Ω is the Rabi strength, \hat{a}^\dagger and \hat{a} are the creation and annihilation operators for the axial mode of motion, $2\phi_+ = \phi_{red} + \phi_{blue}$ and $2\phi_- = \phi_{red} - \phi_{blue}$ are the sum and the difference of the red sideband laser phase ϕ_{red} and the blue sideband laser phase ϕ_{blue} . It can be noted from Eq. (3) that, the setting of ϕ_- determines the axis of the displacement in phase space, the internal state of the ion determines the displacement direction along this axis, and ϕ_+ determines which eigenstates are selected.

It has to be stressed that Eqs. (1) and (2) only hold in the weak coupling limit [32–34]. In the following, we describe the concrete experimental procedure based on the accurate analytic derivation which is valid for arbitrary coupling strength.

After Doppler cooling, sideband cooling, and optical pumping, the internal state of the trapped ion is prepared in $|\psi_i\rangle = |\downarrow\rangle$, and its motional state is initialized to the ground state $|\varphi_i(z)\rangle = (\frac{1}{2\pi\Delta_z^2})^{\frac{1}{4}} \exp(-\frac{z^2}{4\Delta_z^2})$. By setting $\phi_+ = \phi_- = \frac{\pi}{2}$, the spin-dependent displacement Hamiltonian has the form $\hat{H}_d = \eta\Omega\Delta_z\hat{\sigma}_x\hat{p}$ with the momentum operator $\hat{p} = \frac{i\hbar(\hat{a}^\dagger - \hat{a})}{2\Delta_z}$. Application of this Hamiltonian for a duration t generates the entangled state of system and pointer degrees as

$$|\Psi\rangle = \frac{1}{\sqrt{2}}[|+\rangle |\varphi_i(z - g\Delta_z)\rangle - |-\rangle |\varphi_i(z + g\Delta_z)\rangle], \quad (4)$$

where $|+\rangle = \frac{1}{\sqrt{2}}(|\uparrow\rangle + |\downarrow\rangle)$, $|-\rangle = \frac{1}{\sqrt{2}}(|\uparrow\rangle - |\downarrow\rangle)$ and $g = \eta\Omega t$. For the trapped ion system, we can only postselect the state $|\uparrow\rangle$ without destroying the motional

wavepacket as no photons are scattered in the measurement process. However, the postselections of other states can be carried out with the help of appropriate one-qubit rotations. In the experiment, we firstly perform a rotation by 2θ around the y -axis of the Bloch sphere (denoted as $R_y(2\theta)$) on the internal state, which is realized using a laser pulse resonant with the $|\downarrow\rangle \rightarrow |\uparrow\rangle$ transition, then perform the strong projective measurement via state-dependent fluorescence. After retaining only instances with measurement outcome $|\uparrow\rangle$, we effectively realize the postselection with $|\psi_f\rangle = R_y(-2\theta)|\uparrow\rangle = \cos\theta|\uparrow\rangle - \sin\theta|\downarrow\rangle$. Then, the external motion will be left in the state (choosing Δ_z as the unit of \hat{z})

$$|\varphi_f(z)\rangle = \frac{1}{(2\pi)^{\frac{1}{4}}\sqrt{1 - \cos(2\theta)e^{-\frac{g^2}{2}}}} [\cos(\frac{\pi}{4} + \theta)e^{-\frac{(z-g)^2}{4}} - \sin(\frac{\pi}{4} + \theta)e^{-\frac{(z+g)^2}{4}}], \quad (5)$$

with the position displacement

$$\delta_z = \langle\varphi_f(z)|\hat{z}|\varphi_f(z)\rangle = \frac{g}{e^{-\frac{g^2}{2}}\cot(2\theta) - \csc(2\theta)}. \quad (6)$$

It follows from Eqs. (1) and (2) that, the position displacement will reduce to $\delta_z \approx \frac{\langle\psi_f|\hat{\sigma}_x|\psi_i\rangle}{\langle\psi_f|\psi_i\rangle}g = -\cot(\theta)g$ in the weak coupling limit.

The only observable of the trapped ion that can be directly measured via state-dependent fluorescence is $\hat{\sigma}_z$. To proceed with the analysis of the postselected motional state, we use an indirect measurement method for motional wavepacket reconstruction, which was originally proposed in 1995 [35] and has been successfully utilized in the quantum simulation of Dirac equation [36] and random walk [37] in trapped ion system. To measure the marginal probability distribution of the motional state along a line in phase space, we prepare the internal state of the ion in an eigenstate of $\hat{\sigma}_y$ or $\hat{\sigma}_z$, apply a spin-dependent displacement operation that displaces the motional wave function in phase space in a direction orthogonal to the one to be measured for varying amounts of time, followed by a measurement of the changing excitation of the ionic internal state. Then, a Fourier transformation of these measurements yields the marginal probability distribution of the motional wavepacket. Furthermore, the expectation values of the motional quadratures can be obtained by analyzing the slope of the changing excitation in very short time, without a need to reconstruct the full motional wavepacket (see Supplemental Material for details).

In Fig. 2, we experimentally show that a tiny position displacement of 4 Å of the trapped ion can be amplified to 10 nm using the above WVA procedure. In the experiment we use a short spin-dependent displacement pulse with $\Omega = 2\pi \times 19.0$ kHz and $t = 4$ μs to achieve a small position splitting $g \simeq 0.04$. After the internal state postselection using $R_y(-2\theta)|\uparrow\rangle$ with $\theta = 0.02$, a remarkable

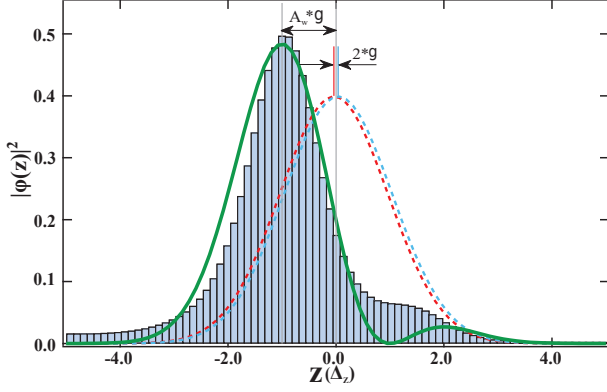


FIG. 2. (Color online) A tiny position displacement of 4 Å of the trapped ion is amplified to 10 nm. The dashed lines indicate the probability distributions of the two weakly displaced wavepackets correlated with the eigenstates of $\hat{\sigma}_x$ in Eq. (4) with $g \simeq 0.04$. The histogram shows the probability distribution of the finally postselected wavepacket reconstructed using the experimental data with $\theta = 0.02$ and the solid line gives the exact theoretical prediction using Eq. (5).

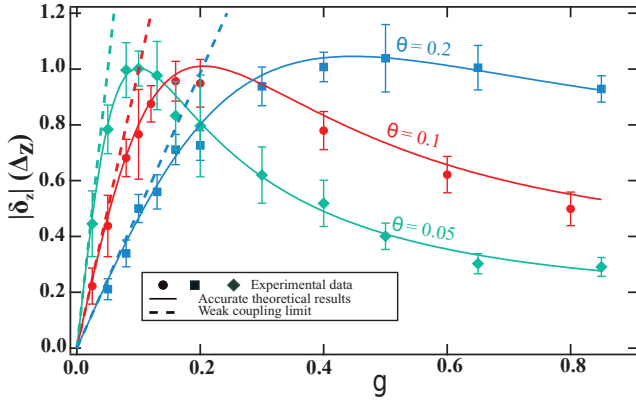


FIG. 3. (Color online) The relation between the magnitude of the amplified position shift $|\delta_z|$ and the original splitting g with different θ . The dashed lines represent the theoretical results in the weak coupling limit where we have $|\delta_z| \approx g|A_w| = g \cot \theta$. The solid lines are the accurate theoretical results. The symbols (•, ■ and ♦) are the experimental data. The error bars represent one standard deviation over the ensemble of postselected events.

WVA effect occurs with the amplified position displacement 10 nm. It should be noted that the weak coupling limit does not hold for this parameter setting and the theoretical amplified position displacement in Fig. 2 is actually obtained from the exact result of Eq. (6).

Through fast measurement of the expectation value of the position operator, we show the relation between the magnitude of the amplified position shift $|\delta_z|$ and the original splitting g with different θ in Fig. 3. In the weak coupling regime defined by $|A_w|g \ll 1$ [38], $|\delta_z|$ increases linearly with g with an amplification factor $|A_w| = \cot \theta$

and the approximate results agree well with the accurate theoretical results and the experimental data. Outside this regime, the amplified position shift has an upper limit $\sim \Delta_z$. With g increasing, the weak measurement regime will transit to the strong measurement regime and the WVA effect disappears.

The WVA procedure with the pure imaginary weak value can also be implemented in our experiment. It has been pointed out that the imaginary weak value has the potential to counteract the time-independent technical noise in quantum metrology applications [15, 39, 40]. By choosing $|\psi_i\rangle = R_x(2\phi)|\downarrow\rangle = \frac{1}{\sqrt{2}}(|+\rangle - e^{i2\phi}|- \rangle)$ and $|\psi_f\rangle = |\uparrow\rangle$, we achieve the pure imaginary weak value $A_w = i \cot \phi$. In this case, the original small position splitting g will result in an amplified moment shift (choosing $\Delta_p = \frac{\hbar}{2\Delta_z}$ as the unit of \hat{p})

$$\delta_p = \frac{g \sin(2\phi)}{e^{\frac{g^2}{2}} - \cos(2\phi)} \quad (7)$$

in phase space, as shown in Fig. 4. In the parameter regime $|A_w|g \ll 1$, the weak coupling approximation is valid and its predictions agree well with the accurate theoretical results and the experimental data. Outside this regime, the amplified momentum shift has an upper limit $\sim \Delta_p$. The extreme sensitivity of WVA to the relative phase of the quantum state in the $\phi \rightarrow 0$ regime may have application in the sensitive estimation of phase with small values.

Now, we propose several possible scenarios of actual sensing applications for our WVA procedure. Firstly, although the above state-dependent force sensed by the ion is engineered using the bichromatic light field, we can replace it with some quantum effects we are interested in for actual sensing scenarios. An interesting example is to observe the tiny momentum kick that an ion receives upon emitting a single photon using this WVA procedure. Suppose we trap an ion which has the ground state $|\downarrow\rangle$ and two metastable excited states $|\uparrow\rangle$ and $|\uparrow'\rangle$. The ion is prepared in the superposition state $\frac{1}{\sqrt{2}}(|\uparrow\rangle + |\uparrow'\rangle)$ and its motional degree of freedom is initialized to the state $|\varphi(z)\rangle$. An appropriately modulated laser pulse, e.g. the rapid adiabatic passage (RAP) pulse [41], can coherently transfer the population from $|\uparrow'\rangle$ to $|\downarrow\rangle$ with the high efficiency and induce the stimulated emission of a single photon. Then the ion will receive a tiny state-dependent recoil kick and the composite quantum state evolves into $\frac{1}{\sqrt{2}}(|\downarrow\rangle \otimes U_{kick}|\varphi(z)\rangle + |\uparrow\rangle \otimes |\varphi(z)\rangle)$, where U_{kick} is the kick acting on the motional wavepacket of the ion. This tiny state-dependent force can be amplified using our WVA procedure, thus to study related quantum phenomena at the single-particle level. Secondly, we can estimate the parameters of classical signals which can be imprinted in the quantum evolution of this procedure. For the pure imaginary weak value case, the final amplified momentum shift is extremely sensitive to the relative

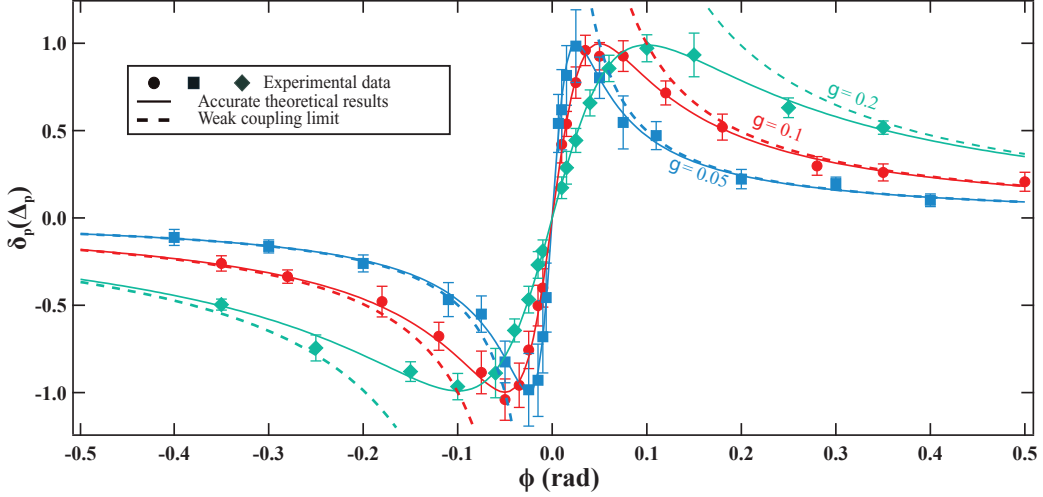


FIG. 4. (Color online) By choosing $|\psi_i\rangle = R_x(2\phi)|\downarrow\rangle$ and $|\psi_f\rangle = |\uparrow\rangle$, we achieve the pure imaginary weak value $A_w = i \cot \phi$ and herein the original small position splitting g will result in an amplified momentum shift δ_p in phase space. The dashed lines represent the theoretical results in the weak coupling limit where we have $\delta_p \approx g \text{Im}(A_w) = g \cot \phi$. The solid lines are the accurate theoretical results. The symbols (\bullet , \blacksquare and \blacklozenge) are the experimental data. The error bars represent one standard deviation over the ensemble of postselected events.

phase of the preselected superposition state. If this phase is induced by an unknown weak magnetic field signal (the Zeeman splitting of the ion's electronic states can encode a relative phase in the superposition state), we can infer the information of the measured magnetic field from the value of the amplified momentum shift. Besides the magnetic field sensing, using the sensitive dependence of the WVA effect on RF signals driving the AOM, we can also use this configuration to sense the tiny change for parameters of RF signals.

It has been verified that the WVA procedure can obtain almost all the Fisher information using only the small portion of surviving postselected events [16]. The WVA procedures can possibly afford a benefit over conventional ones because of the fewer consumption of the detection resource. For optical WVA, the photons failing in the postselection step will not arrive at the detector, which will alleviate the limitation of detector saturation [19]. Actually, for the trapped ion system, the most time-consuming step is the motional wavepacket analysis, and our atomic WVA procedure will consume fewer detection resource than conventional procedures in this system. Specifically, in the proceeding of our procedure, if the postselection step fails, we will cancel the very time-consuming process of analyzing the motional wavepacket and move directly to the next experimental cycle. Thus, compared with conventional methods with no postselection, our procedure will consume fewer resource of detection time in average for acquiring the same information.

Considering that WVA has become an important part of the standard toolbox in the modern field of quantum control, this first demonstration of atomic WVA suggests

interesting physics also from the fundamental perspectives. Our work has demonstrated the high operational flexibility in the atomic WVA procedure. The interaction strength between the measured system degree and the measuring pointer degree can be tuned over a wide range, and their coupling pattern can be manipulated by adjusting the experimental parameters. Combined with the easily tailored pointer state, which can be prepared in various nonclassical motional states (e.g. Fock states, squeezed states, even two-mode NOON states [42, 43]), and the ability to coherently manipulate several tens of ions [44], our approach allows fully exploration of the peculiarities of WVA.

In conclusion, we present the first experimental realization of fully atomic WVA using the trapped ion system. The remarkable amplification of motional displacement and the extreme sensitivity of WVA to the relative phase of the quantum state are demonstrated in our experiment. The good agreement between the calculated and experimental results shows the trapped ion as a favorable platform for WVA research. The good scalability and flexible controllability of trapped ion system make it an important complement to optics in this research area. More importantly, our experiment makes the first step towards the study of atomic WVA and has much potential in the studies of fundamental quantum mechanics and quantum metrology.

This work was supported by the National Basic Research Program of China under Grant No.2016YFA0301903, the National Natural Science Foundation of China under Grant Nos.11174370, 11304387, 61632021, 11305262, and 11574398, and the

Research Plan Project of National University of Defense Technology under Grant No. ZK16-0304.

* These authors contributed equally to this paper.

† Corresponding author: weiwu@nudt.edu.cn

‡ Corresponding author: pxchen@nudt.edu.cn

- [1] V. B. Braginsky, F. Y. Khalili, and K. S. Thorne, *Quantum measurement* (Cambridge University Press, Cambridge, 1995).
- [2] J. V. Neumann, *Mathematical Foundations of Quantum mechanics* (Springer Press, Berlin, 1932).
- [3] Y. Aharonov, D. Z. Albert, and L. Vaidman, Phys. Rev. Lett. **60**, 1351 (1988).
- [4] J. Dressel, M. Malik, F. M. Miatto *et al.*, Rev. Mod. Phys. **86**, 307 (2014).
- [5] G. C. Knee, J. Combes, C. Ferrie, and E. M. Gauger, Quantum Measurements and Quantum Metrology, **3**, 32 (2016).
- [6] O. Hosten, and P. Kwiat, Science **319**, 787 (2008).
- [7] P. B. Dixon, D. J. Starling *et al.*, Phys. Rev. Lett. **102**, 173601 (2009).
- [8] M. Hallaji, A. Feizpour, G. Dmochowski *et al.*, Nat. Phys. **13**, 540 (2017).
- [9] G. S. Thekkadath, L. Giner, Y. Chalich *et al.*, Phys. Rev. Lett. **117**, 120401 (2016).
- [10] M. M. Weston, M. J. W. Hall, M. S. Palsson *et al.*, Phys. Rev. Lett. **110**, 220402 (2013).
- [11] W. J. Zou, Y. H. Li, S. C. Wang *et al.*, Phys. Rev. A **95**, 042342 (2017).
- [12] C. Ferrie, and J. Combes, Phys. Rev. Lett. **112**, 040406 (2014).
- [13] L. J. Zhang, A. Datta, and I. A. Walmsley, Phys. Rev. Lett. **114**, 210801 (2015).
- [14] A. Feizpour, X. Xing, and A. M. Steinberg, Phys. Rev. Lett. **107**, 133603 (2011).
- [15] A. N. Jordan, J. M. Rincón, and J. C. Howell, Phys. Rev. X **4**, 011031 (2014).
- [16] G. I. Viza, J. M. Rincón *et al.*, Phys. Rev. A **92**, 032127 (2015).
- [17] J. Harris, R. W. Boyd, and J. S. Lundeen, Phys. Rev. Lett. **118**, 070802 (2017).
- [18] L. Vaidman, arXiv:1402.0199.
- [19] L. Vaidman, Phil. Trans. Roy. Soc. A **375**, 20160395 (2017).
- [20] A. Romito, Y. Gefen, and Y. M. Blanter, Phys. Rev. Lett. **100**, 056801 (2008).
- [21] O. Zilberberg, A. Romito, and Y. Gefen, Phys. Rev. Lett. **106**, 080405 (2011).
- [22] J. P. Groen, D. Ristè *et al.*, Phys. Rev. Lett. **111**, 090506 (2013).
- [23] D. Lu, A. Brodutch *et al.*, New J. Phys. **16**, 053015 (2014).
- [24] T. Denkmayr, H. Geppert *et al.*, Phys. Rev. Lett. **118**, 010402 (2017).
- [25] I. Shomroni, O. Bechler, S. Rosenblum, and B. Dayan, Phys. Rev. Lett. **111**, 023604 (2013).
- [26] M. Zhang, and S. Y. Zhu, Phys. Rev. A **92**, 043825 (2015).
- [27] G. Aranedo, S. Walser *et al.*, Nat. Phys. **15**, 17 (2019).
- [28] N. Herschbach, K. Pyka *et al.*, Appl. Phys. B **107**, 891 (2012).
- [29] I. Baumgart, J. M. Cai *et al.*, Phys. Rev. Lett. **116**, 240801 (2016).
- [30] A. Aiello and J. P. Woerdman, Opt. Lett. **33**, 1437 (2008).
- [31] R. Jozsa, Phys. Rev. A **76**, 044103 (2007).
- [32] X. Zhu, Y. Zhang *et al.*, Phys. Rev. A **84**, 052111 (2011).
- [33] L. Vaidman, A. Ben-Israel *et al.*, Phys. Rev. A **96**, 032114 (2017).
- [34] J. Dziewior, L. Knips *et al.*, arXiv:1804.05400.
- [35] S. Wallentowitz and W. Vogel, Phys. Rev. Lett. **75**, 2932 (1995).
- [36] R. Gerritsma, G. Kirchmair *et al.*, Nature **463**, 68 (2010).
- [37] F. Zähringer, G. Kirchmair *et al.*, Phys. Rev. Lett. **104**, 100503 (2010).
- [38] I. M. Duck, P. M. Stevenson, and E. C. G. Sudarshan, Phys. Rev. D **40**, 2112 (1989).
- [39] J. M. Rincón, W. T. Liu *et al.*, Phys. Rev. Lett. **116**, 100803 (2016).
- [40] W. T. Liu, J. M. Rincón *et al.*, Opt. Lett. **42**, 903 (2017).
- [41] B. T. Torosov, S. Guérin *et al.*, Phys. Rev. Lett. **106**, 233001 (2011).
- [42] D. M. Meekhof, C. Monroe *et al.*, Phys. Rev. Lett. **76**, 1796 (1996).
- [43] J. Zhang, M. Um *et al.*, Phys. Rev. Lett. **121**, 160502 (2018).
- [44] C. Kokail, C. Maier *et al.*, Nature **569**, 355 (2019).

Supplemental Material for “ Experimental Demonstration of Fully Atomic Weak Value Amplification ”

Chun-Wang Wu,^{1,2,*} Jie Zhang,^{1,2,*} Yi Xie,^{1,2} Bao-Quan
Ou,^{1,2} Ting Chen,^{1,2} Wei Wu,^{1,2,†} and Ping-Xing Chen^{1,2,‡}

¹*Department of Physics, College of Liberal Arts and Sciences,
National University of Defense Technology, Changsha 410073, Hunan, China.*

²*Interdisciplinary Center for Quantum Information,*

National University of Defense Technology, Changsha 410073, Hunan, China.

(Dated: June 21, 2019)

In this supplementary material we describe the trapped ion system in more detail, discuss the postselection step and the calibration of the experimental parameters, and finally illustrate the wavepacket reconstruction method along with the data analysis for the measurement of $\langle \hat{z} \rangle$ and $\langle \hat{p} \rangle$.

EXPERIMENTAL SETUP

A single ion $^{40}\text{Ca}^+$ trapped in a blade-shaped linear Paul trap is used in the experiment. In the first part of the experimental sequence, all the motional modes of the single ion are cooled down to a phonon number of about 20 using Doppler cooling method with lasers at 397 and 866 nm. The oscillator we use for our experiment is the axial mode, which has a secular frequency of around $\omega_z/(2\pi) = 1.41$ MHz. After Doppler cooling, the axial mode is cooled further to the motional ground state with the resolved sideband cooling approach [1]. A narrow linewidth laser at 729 nm is used to coherently couple the qubit which we choose the energy levels $S_{1/2}(m_J = -1/2)$ and $D_{5/2}(m_J = -1/2)$ as $|\downarrow\rangle$ and $|\uparrow\rangle$ respectively. The whole setup for controlling the qubit is shown in Fig. 1. The power of 729 nm laser beam is stabilized by using acousto-optical modulator (AOM) 1. AOM 2 is used to shift up the laser frequency by 80 MHz and modulate the bichromatic light field for the spin-dependent force. The amplitude and frequency of the beam are controlled by AOM 3, which has a double pass optical configuration and is driven by an RF source with frequency 270 MHz. It is also used as a switch for generation of laser pulses in the experimental sequence. The qubit transition is isolated by a gap of 8.8 MHz from its nearest internal state transitions with a magnetic field of 5.2 G. The beam goes through the two end-caps with almost 0 degree with respect to z axis of the trap resulting in a Lamb-Dicke parameter of $\eta \approx 0.08$ as shown in Fig. 1. Optical pumping to $|\downarrow\rangle$ is realized using a combination of left-handed circularly polarized light at 397 nm, and linearly polarized light at 866 nm and 854 nm. The internal state of the ion is read by using the electron shelving technique with a detection time of 300 μs . The heating rate of the axial motional mode is about 70 quanta per second, and the coherence time of the Fock state superposition $(|0\rangle + |1\rangle)/\sqrt{2}$ has been measured to be about 5.0 ms. Due to the large magnetic fluctuations induced by the AC-power line, we trigger the experimental cycles at 50 Hz and the coherence time of the qubit

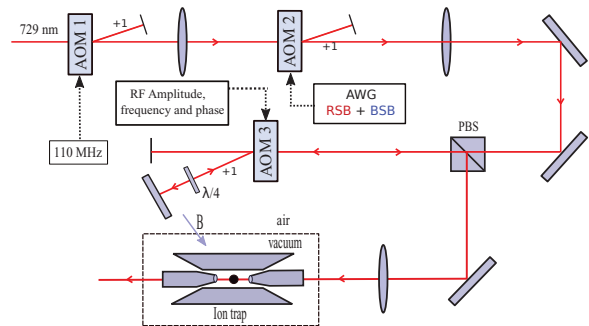


FIG. 1. (Color online) The trap geometry and optical setup in our experiment. AOM 1 is used for power stabilization of the 729 nm laser beam. AOM 2 creates the required bichromatic laser field when it is supplied with two frequencies of RF signals that differ by $2\omega_z$. The RF signals are generated by an arbitrary waveform generator (AWG). AOM 3 controls the overall frequency and amplitude of the 729 nm laser beam.

has been measured using Rasmey fringe to be around 1.1 ms.

HERALDED DETECTION

The internal state detection via application of lasers at 397 nm and 866 nm is used for postselection of the motional wavepacket. The wavepacket is retained if the ion is in $|\uparrow\rangle$ and no fluorescence photons should be detected, while it is destroyed if the ion is in $|\downarrow\rangle$ and a certain amount of photons should be gathered. Since the coherence time is limited, we want to use the shortest detection time for the postselection to avoid decoherence. The detection time in our experiment is chosen as 120 μ s and we distinguish the ion's electronic states based on a predetermined threshold for the gathered photons. With a detection time of 120 μ s, the detection error is less than 0.003% for an ion which is measured to be in $|\uparrow\rangle$. As stated in Ref. [2], such low error is of the similar size to other sources of error in the experiment.

CALIBRATION OF THE DISPLACED OPERATION

Making sure that we apply an accurate displacement on the motional ground state is the critical step in our experiment. The displacement operation can be realized by a single bichromatic laser pulse which creates a Schrödinger cat state between the electronic states and the motional states. By applying the spin-dependent displacement operator for a time t on the initial state $|\downarrow\rangle|0\rangle$, where $|0\rangle$ is the motional ground state, we get the entangled state

$$|\Psi\rangle = D(\alpha)|\downarrow\rangle|0\rangle = \frac{1}{\sqrt{2}}(|+\rangle|\alpha\rangle - |-\rangle|-\alpha\rangle), \quad (1)$$

where $|+\rangle = \frac{1}{\sqrt{2}}(|\uparrow\rangle + |\downarrow\rangle)$, $|-\rangle = \frac{1}{\sqrt{2}}(|\uparrow\rangle - |\downarrow\rangle)$, and $D(\alpha) = e^{\frac{2\alpha\Delta_z\hat{\sigma}_x\hat{p}}{i\hbar}}$. The displacement $\alpha = \eta\Omega t/2$ is proportional to the Lamb-Dicke parameter η , the coupling strength Ω , and the bichromatic pulse duration t . For the trapped ion, the only observable we can measure is $\hat{\sigma}_z$, and a projective measurement on $|\Psi\rangle$ returns the probability of ion in $|\uparrow\rangle$

$$p_{\uparrow} = \frac{1}{2}(1 + \langle\hat{\sigma}_z\rangle) = \frac{1}{2}(1 - e^{-2|\alpha|^2}). \quad (2)$$

Note that Ω means both the coupling strengths of red and blue sidebands, hence the intensities of the two RF signals driving AOM 2 are required to be equal. We perform the uniformity calibration of coupling strengths for the red sideband and blue sideband lasers by checking if the probability of $|\uparrow\rangle$ reaches 0.5 when the ground state wavepacket totally splits into two parts. Fig. 2 shows an experimental measurement of p_{\uparrow} after evolution under the balanced bichromatic field along with the theoretical simulation of Eq. (2) for $\eta = 0.08$ and $\Omega = 2\pi \times 150$ kHz.

To demonstrate WVA, We also need to calibrate the small displacement α as a function of the bichromatic pulse length by measuring the phonon number of the ion, which follows the Poisson distribution and has the average $\bar{n} = |\alpha|^2$. Experimentally we choose a low coupling strength for the bichromatic light field and probe the average phonon number of the ion by applying the pulse for varying amounts of time, and the corresponding results are shown in Fig. 3. The coupling strength used in the experiment is then determined to be $\Omega \approx 2\pi \times 19.0$ kHz.

WAVEPACKET RECONSTRUCTION AND DISPLACEMENT MEASUREMENT IN PHASE SPACE

To obtain the wavepacket probability distribution, we apply a state-dependent displacement operation $\hat{U}_z = \exp(-ik\hat{z}\hat{\sigma}_x/2)$ to the measured quantum state and then

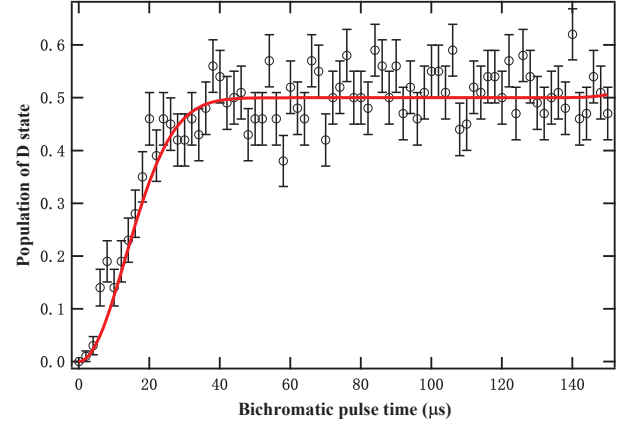


FIG. 2. (Color online) Uniformity calibration of coupling strengths for the red sideband and blue sideband lasers. The red line is a plot of Eq. (2) with parameters $\eta = 0.08$ and $\Omega = 2\pi \times 150$ kHz. The black dots indicate the experimental measurement of $|\uparrow\rangle$ at chosen times.

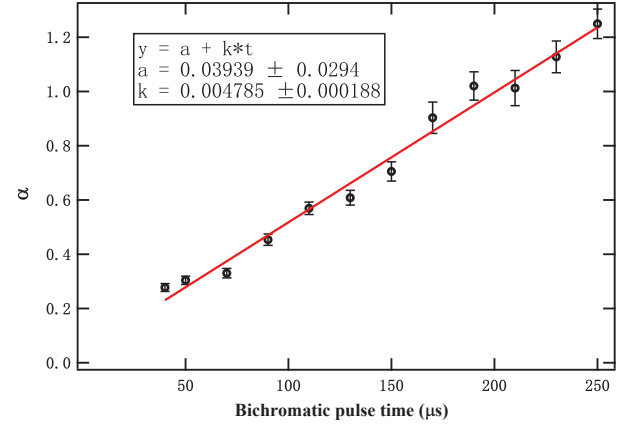


FIG. 3. (Color online) Calibration of the displacement α as a function of the bichromatic pulse time with the low coupling strength. The black dots indicate α obtained from measurement of the average phonon number \bar{n} . The red line denotes the fitting of data points and the corresponding coupling strength of the bichromatic field is determined to be $\Omega \approx 2\pi \times 19.0$ kHz.

the following measurement of $\hat{\sigma}_z$ effectively returns the measurement outcome of the observable

$$\hat{O}(k) = \hat{U}_z^\dagger \hat{\sigma}_z \hat{U}_z = \cos(k\hat{z})\hat{\sigma}_z + \sin(k\hat{z})\hat{\sigma}_y, \quad (3)$$

where $k = \eta\Omega t/\Delta_z$, and $\Omega \approx 2\pi \times 70$ kHz. If we prepare the internal state of the ion to be the eigenstate of $\hat{\sigma}_z$ with eigenvalue +1, then we have $\langle\hat{O}(k)\rangle = \langle\cos(k\hat{z})\rangle$. Similarly, we have $\langle\hat{O}(k)\rangle = \langle\sin(k\hat{z})\rangle$ if the eigenstate of $\hat{\sigma}_y$ with eigenvalue +1 is prepared. Theoretically we can get the probability density $|\varphi(z)|^2$ by using Fourier transformation of $\langle\cos(k\hat{z})\rangle + i\langle\sin(k\hat{z})\rangle$ [3], however the finite experimental cycles can not afford enough infor-

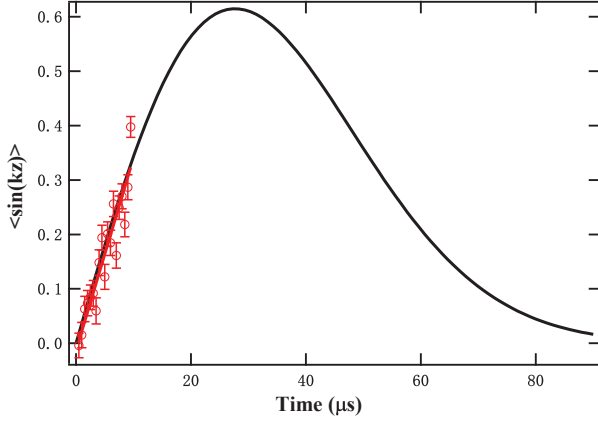


FIG. 4. (Color online) Data analysis for obtaining the average displacement. The black curve denotes the full simulation of $\langle \sin(k\hat{z}) \rangle$ with parameters $g = 0.2$ and $\theta = 0.2$. The red cycles are experimental data. The red line shows the weighted fitting of data points for extracting $\langle \hat{z} \rangle$.

mation for this method. Instead we use a constrained least-square optimization method based on convex optimization [4] as stated in Ref. [5]. In this method the position space is first discretized by a suitable set of points z_i and probability distributions of $p(z_i)$ can be searched by minimizing the function

$$F = \sum_k \left(\sum_i p(z_i) \cos(kz_i) - C_k \right)^2 + \sum_k \left(\sum_i p(z_i) \sin(kz_i) - S_k \right)^2, \quad (4)$$

where C_k and S_k are the experimental results of $\langle \cos(k\hat{z}) \rangle$ and $\langle \sin(k\hat{z}) \rangle$ respectively.

In this technique we also need to apply additional constraints. Firstly, the probability of the position points meet the conditions $0 \leq p(z_i) \leq 1$ and $\sum_i p(z_i) = 1$. Secondly, $p'(z)$, the differentiation of the probability distribution function $p(z)$ with respect to position z , should be bounded by the kinetic energy of the ion [5]

$$\frac{\hbar^2}{8m} \int_{-\infty}^{\infty} dz \frac{p'(z)^2}{p(z)} \leq \left\langle \frac{\hat{p}^2}{2m} \right\rangle. \quad (5)$$

For obtainment of the value of $\langle \hat{p}^2 \rangle$, we only need to adjust the phase of the bichromatic laser pulse to realize $\hat{U}_p = \exp(-ik\hat{p}\hat{\sigma}_x/2)$, and finally calculate $\langle \hat{p}^2 \rangle = d^2/dk^2 \langle \hat{O}(k) \rangle$.

Besides the wavepacket, we are also concerned about the average shifts of the wavepacket. From Eq. (3) we can obtain $\frac{d}{dk} \langle \hat{O}(k) \rangle|_{t=0} = \langle \hat{z}\hat{\sigma}_y \rangle$, therefore the average position displacement $\langle \hat{z} \rangle$ can be measured by preparing the internal state to be the eigenstate of $\hat{\sigma}_y$. Experimentally the state of the ion is $|\uparrow\rangle$ after postselection, we need to apply a $\pi/2$ carrier transition laser pulse to coherently prepare the internal state in $(|\downarrow\rangle + i|\uparrow\rangle)/\sqrt{2}$. Afterwards we apply the operation \hat{U}_z and detect $\langle \sin(k\hat{z}) \rangle$ for a short length of time (10 μ s in the experiment), and $\langle \hat{z} \rangle$ can be extracted by fitting the data points with a linear model as shown in Fig. 4. The same method can be used for the measurement of $\langle \hat{p} \rangle$, the only difference here is the operation we apply after postselection detection is $\hat{U}_p = \exp(-ik\hat{p}\hat{\sigma}_x/2)$.

Since the wavepacket reconstruction pulses are applied after postselection, the success rates of postselection are different from point to point in the experiment and it is necessary to consider the different contributions to the fitting error for different data points. Hence, we use the weighted fitting method instead of the regular fitting method to fit the data, the standard deviation derived from quantum projection noise of each data point is used as the weighting parameter [6]. Fig. 4 shows an example of data analysis for measuring $\langle \hat{z} \rangle$ with parameters $g = 0.4$ and $\theta = 0.2$.

* These authors contributed equally to this paper.

† Corresponding author: weiwu@nudt.edu.cn

‡ Corresponding author: pxchen@nudt.edu.cn

- [1] C. Roos, T. Zeiger, H. Rohde, H. C. Nägerl, J. Eschner, D. Leibfried, F. Schmidt-Kaler, and R. Blatt, Phys. Rev. Lett. **83**, 4713 (1999).
- [2] D. Kienzler, C. Flühmann, V. Negnevitsky, H.-Y. Lo, M. Marinelli, D. Nadlinger, and J. P. Home, Phys. Rev. Lett. **116**, 140402 (2016).
- [3] R. Gerritsma, G. Kirchmair *et al.*, Nature **463**, 68 (2010).
- [4] M. Grant, S. Boyd, and Y. Ye, Web page and software available at <http://stanford.edu/boyd/cvx> (2015).
- [5] F. Zähringer, G. Kirchmair *et al.*, Phys. Rev. Lett. **104**, 100503 (2010).
- [6] C. Croarkin, P. Tobias, J. Filliben, B. Hembree, W. Guthrie, et al., NIST/SEMATECH, July. Available online: <http://www.itl.nist.gov/div898/handbook> (2006).